INSTITUTE OF PHYSICS PUBLISHING PLASMA PHYSICS AND CONTROLLED FUSION

Plasma Phys. Control. Fusion **44** (2002) 567–578 PII: S0741-3335(02)31687-7

# Measurements with an emissive probe in the CASTOR tokamak

**Roman Schrittwieser[1,6], Jiří Adámek[2], Petru Balan[1], Martin Hron[2], Codrina Ioniţă[1], Karel Jakubka[2], Ladislav Kryška[2], Emilio Martines[3], Jan Stöckel[2], Milan Tichy[4] and Guido Van Oost[5]**

[1] Institute for Ion Physics, University of Innsbruck, Innsbruck, Austria
[2] Institute of Plasma Physics, Association EURATOM/IPP.CR, Academy of Sciences of the Czech Republic, Prague, Czech Republic
[3] Consorzio RFX, Associazione EURATOM-ENEA sulla Fusione, Padova, Italy
[4] Charles University in Prague, Faculty of Mathematics and Physics, Prague, Czech Republic
[5] Department of Applied Physics, Ghent University, Ghent, Belgium

E-mail: roman.schrittwieser@uibk.ac.at

Received 7 December 2001
Published 22 April 2002
Online at stacks.iop.org/PPCF/44/567

**Abstract**

An emissive probe has been used in the edge region of the CASTOR tokamak in order to test the possibility of direct measurements of the plasma potential. The difference between the floating potential of a cold probe and that of an emissive probe has been found to be approximately 1.3 times the electron temperature, which is less than predicted by the probe theory. Several possible reasons to explain this discrepancy are offered, such as secondary electron emission, uncertainties in the ion temperature, different collecting areas for electrons and ions, etc. The possible impact of a space charge formed by the emitted electrons is also discussed.

## 1. Introduction

Particle and energy confinement in magnetized plasmas are strongly influenced by electric fields and their fluctuations [1]. Electric fields are determined by gradients of the plasma potential. In the edge region of fusion devices, the plasma potential is usually deduced from the floating potential measured by Langmuir probes. The difference between the floating potential $V_{\mathrm{fl}}$ and the plasma potential $\Phi$ is a function of electron and ion temperatures and possibly also other parameters:

$$V_{\mathrm{fl}} = \Phi - f(T_{\mathrm{i}}, T_{\mathrm{e}}, \ldots). \tag{1}$$

This technique is comparatively simple and provides the local information with a satisfactory temporal resolution.

[6] Author to whom correspondence should be addressed.

  

However, this indirect evaluation is potentially subject to errors, due to the uncertainty in the knowledge of the function $f$ and of its variables. This is particularly true for turbulence-induced particle fluxes, which require the knowledge of the fluctuating electric field [2]. These complications could be circumvented using a technique able to directly measure the plasma potential. One suitable technique for the edge region of small fusion devices is the *emissive* probe, which is often used for low-temperature plasma diagnostics. This is an actively heated probe, which emits electrons. As long as such a probe is not heated, it will be called *cold* probe.

In this paper we present measurements of the floating potential profile of an emissive probe in the boundary plasma of a tokamak. In section 2 we specify the function $f$ introduced in equation (1). Section 3 explains the principle of emissive probes. Section 4 describes the experimental apparatus. In section 5 the results of the experiments, performed on the CASTOR tokamak, are presented. Section 6 discusses the results, while the conclusions are drawn in section 7.

## 2. Floating potential of a cold probe

The interpretation of the probe measurements in tokamaks is usually based on the elementary Langmuir probe theory, which provides the relation between the plasma and the floating potential, assuming a Maxwellian electron velocity distribution. The magnetic field is taken into account only by reducing the effective collecting area of the probe. If the probe voltage $V_\mathrm{p}$ (measured with respect to a reference electrode) biases the probe negatively with respect to the plasma potential $\Phi$, the probe current $I_\mathrm{p}$ is the sum of the electron and the ion currents:

$$I_\mathrm{p} = I_\mathrm{is}(1+\gamma_\mathrm{i}) - I_\mathrm{es}(1-\gamma_\mathrm{e})\exp\left[-\frac{e(\Phi - V_\mathrm{p})}{k_\mathrm{B}T_\mathrm{e}}\right], \tag{2}$$

where $I_\mathrm{es}$ and $I_\mathrm{is}$ are the electron and ion saturation currents, $k_\mathrm{B}$ is the Boltzmann constant and $T_\mathrm{e}$ is the electron temperature. The coefficients $\gamma_\mathrm{e}$ and $\gamma_\mathrm{i}$ characterize the contribution of the secondary electron emission to the probe current induced by electrons and ions, respectively (a more detailed discussion is given in section 6). In a strongly magnetized, fully ionized tokamak plasma edge, equation (2) is strictly valid only for probe potentials lower than the floating potential (see e.g. [3]). At the floating potential $V_\mathrm{p} = V_\mathrm{fl}$ the total probe current $I_\mathrm{p}$ equals zero. Then, the normalized difference between the floating and the plasma potential is

$$\Delta = \frac{e(\Phi - V_\mathrm{fl})}{k_\mathrm{B}T_\mathrm{e}} = \ln\left(\frac{(1-\gamma_\mathrm{e})}{(1+\gamma_\mathrm{i})}\frac{I_\mathrm{es}}{I_\mathrm{is}}\right). \tag{3}$$

The electron saturation current $I_\mathrm{es}$ is given by the random thermal current density $j_\mathrm{es}$ multiplied by the probe collecting area for electrons $A_\mathrm{e}$:

$$I_\mathrm{es} = A_\mathrm{e} j_\mathrm{es} = A_\mathrm{e}\frac{1}{4}en\sqrt{\frac{8k_\mathrm{B}T_\mathrm{e}}{\pi m_\mathrm{e}}}, \tag{4}$$

with $m_\mathrm{e}$ being the electron mass.

The ion saturation current in a pure, fully ionized hydrogen plasma is [4]

$$I_\mathrm{is} = A_\mathrm{i} j_\mathrm{is} = A_\mathrm{i} en\sqrt{\frac{k_\mathrm{B}(T_\mathrm{e}+T_\mathrm{i})}{m_\mathrm{p}}}, \tag{5}$$

where $A_\mathrm{i}$ is the collection area for ions, $n$ is the electron density at the edge of the probe sheath, $T_\mathrm{i}$ is the ion temperature and $m_\mathrm{p}$ is the proton mass.

At high magnetic fields, there can be a considerable difference in the effective collecting areas for electrons and ions due to the large difference between the ion and electron gyro-radii $\rho_{i,e}$. In the case of a cylindrical probe, $\rho_{i,e}$ has to be compared to the probe radius $r_p$.

Neglecting secondary electron emission, for a hydrogen plasma, equation (3) reads

$$\Delta = \ln\left(\frac{A_e}{A_i}\sqrt{\frac{T_e}{T_e + T_i}}\sqrt{\frac{m_p}{2\pi m_e}}\right). \tag{6}$$

At modest magnetic fields (like in CASTOR) $\rho_i \geqslant r_p$ holds for ions, whereas the contrary is valid for electrons, i.e. $\rho_e \ll r_p$. Therefore in the surroundings of the probe, ions can be considered unmagnetized whereas electrons are strongly magnetized. Thus for ions we have to take into account the entire surface of the probe wire as effective collecting area, while electrons 'see' only the cross-section of the probe wire.

## 3. Emissive probe

An emissive probe usually consists of a small loop of tungsten wire, heated by an external DC current so that the tungsten wire becomes emissive [5–10]. It is worth noting that even usual cold probes can become self-emissive in hot plasmas due to heating by the high-energy fluxes [11].

The probe loop used in our experiment consists of a tungsten wire with a radius $r_p$ and a length $l_p$. Following the arguments above, for ions the effective collecting area is the total surface of the wire, i.e. $A_i = 2r_p\pi l_p$. For electrons, however, flowing from both sides towards the probe wire, the effective collecting area is given by twice the cross-section of the wire, i.e. $A_e = 4r_p l_p$, and $A_e/A_i = 2/\pi$. Only for the extreme case where the loop is perfectly aligned to the magnetic field lines, the area would reduce to $A_e = 2r_p l_p$ since the inner side of the loop wire would be shaded by the opposite outer sides of the wire.

If the probe is not heated, for $\gamma_e = \gamma_i = 0$ and $A_e/A_i \cong 2/\pi$, equation (6) becomes

$$\Delta = \ln\left(\frac{2}{\pi}\sqrt{\frac{T_e}{T_e + T_i}}\sqrt{\frac{m_p}{2\pi m_e}}\right). \tag{7}$$

For $T_e = T_i$, the value of $\Delta$ is equal to 2.04, and from equations (4) and (5) we find that $I_{es}/I_{is} \cong 7.7$.

The saturated thermal electron emission current density $j_{em}$ is given by the Richardson–Dushman formula [12]:

$$j_{em} = A^* T_w^2 \exp\left[-\frac{eW_w}{k_B T_w}\right]. \tag{8}$$

In this expression $A^*$ is the Richardson constant, equal to $7.4 \times 10^5\ \mathrm{A\,m^{-2}\,K^{-2}}$ for tungsten, and $T_w$ and $W_w$ are the temperature and the work function of the wire material, respectively. $W_w$ is 4.55 eV for tungsten.

In order to derive a quantitative expression for the potential of a floating emissive probe, we will discuss two cases: one with the emission current independent of $V_p$, and the other by taking into account space charge effects by the emitted electrons.

### *3.1. Saturated emission*

The electrons emitted by the probe yield a current, which adds to the electron and ion currents coming from the plasma. The total probe current is therefore

$$I_p = I_{is}(1 + \gamma_i) - I_{es}(1 - \gamma_e)\exp\left[-\frac{e(\Phi - V_p)}{k_B T_e}\right] + I_{em}, \tag{9}$$

where $I_{em} = j_{em}A_{em}$ is the emission current, $A_{em}$ is the effective emitting surface, which is supposed to be equal to the total surface of the probe wire; therefore $A_{em} = A_i$. In the following simple analysis, we assume that $I_{em}$ is independent of the probe potential as long as this potential is negative with respect to the plasma potential. The normalized difference between the floating and the plasma potentials for this case will be denoted by $\Delta_{em}$, which, following the approach of section 2, can be written as

$$\Delta_{em} = \frac{e(\Phi - V_{fl}^{em})}{k_B T_e} = \ln\left(\frac{I_{es}(1-\gamma_e)}{I_{is}(1+\gamma_i) + I_{em}}\right). \tag{10}$$

$V_{fl}^{em}$ denotes the floating potential depending on the emission current.

This expression shows that by increasing the emission, the probe floating potential theoretically approaches the plasma potential ($\Delta_{em} \to 0$). The probe attains the plasma potential for

$$\frac{I_{es}(1-\gamma_e)}{I_{is}(1+\gamma_i) + I_{em}} = 1. \tag{11}$$

After insertion of equations (4) and (5), and again under the assumption that $A_e/A_i \cong 2/\pi$, equation (11) becomes

$$\frac{I_{em}}{I_{is}} = \frac{2}{\pi}\sqrt{\frac{T_e}{T_e + T_i}}\sqrt{\frac{m_p}{2\pi m_e}} - 1. \tag{12}$$

For $T_e = T_i$, we can calculate that the ratio of emission current to ion saturation current, necessary to make the floating potential of the probe equal to the plasma potential, is $I_{em}/I_{is} \cong 6.7$. If the probe temperature is further increased, part of the emitted electrons will be reflected by the plasma, keeping the probe at the plasma potential.

We note that by neglecting the difference between the effective collecting areas for electrons and ions, i.e. by putting $A_e/A_i \cong 1$, we obtain $\Delta \cong 2.49$, $I_{es}/I_{is} \cong 12$ and $I_{em}/I_{is} \cong 11$.

### *3.2. Space charge limited emission*

The treatment above is valid as long as space charge effects by the emitted electrons can be neglected. As pointed out recently by Reinmüller [13] and Ye and Takamura [14], for strong electron emission a negative space charge might form around the emissive probe, which would lead to a modification of the floating potential of the probe with respect to the case discussed in section 3.1.

In order to get a rough quantitative idea about this effect, we make the following consideration. Suppose that the emission current is controlled by space charge effects; in equation (9) we replace $I_{em}$ by the Child–Langmuir expression [15]:

$$I_{CL}(V_p) = A_{em}\frac{4\varepsilon_0}{9}\left(\frac{2e}{m_e}\right)^{1/2}\frac{(\Phi - V_p)^{3/2}}{d^2}, \tag{13}$$

where $d$ is the sheath thickness. In the case of an emissive probe in a plasma, $d$ is proportional to the Debye length, $d = k\lambda_{De}$. With this, at the floating potential $V_{fl}^{CL}$, equation (13) becomes

$$I_{CL}(V_{fl}^{CL}) = A_{em}\frac{4n_e e}{9k^2}\left(\frac{2k_B T_e}{m_e}\right)^{1/2}\left[\frac{e(\Phi - V_{fl}^{CL})}{k_B T_e}\right]^{3/2}. \tag{14}$$

Equating the total probe current (neglecting secondary electron emission) to zero, equation (9) for this case becomes

$$0 = I_{is} - I_{es}\exp\left[\frac{e(\Phi - V_{fl}^{CL})}{k_B T_e}\right] + I_{CL}(V_{fl}^{CL}). \tag{15}$$

We emphasize that in this case $V_{\mathrm{fl}}^{\mathrm{CL}}$ does not depend on the emission current.

In analogy to equation (3), we define

$$\Delta_{\mathrm{CL}} = \frac{e(\Phi - V_{\mathrm{fl}}^{\mathrm{CL}})}{k_{\mathrm{B}} T_{\mathrm{e}}}. \tag{16}$$

For further analysis it will be useful to normalize the Child–Langmuir current to the electron saturation current $I_{\mathrm{es}}$, given by equation (4). Therewith we obtain

$$\frac{I_{\mathrm{CL}}}{I_{\mathrm{es}}} = \frac{A_{\mathrm{em}}}{A_{\mathrm{e}}} \frac{2\sqrt{\pi}}{9k^2} \Delta_{\mathrm{CL}}^{3/2} \equiv K \Delta_{\mathrm{CL}}^{3/2}, \tag{17}$$

with

$$K \equiv \frac{A_{\mathrm{em}}}{A_{\mathrm{e}}} \frac{2\sqrt{\pi}}{9k^2}.$$

Using equations (16) and (17), equation (15) becomes

$$\frac{I_{\mathrm{is}}}{I_{\mathrm{es}}} + K \Delta_{\mathrm{CL}}^{3/2} - \exp(-\Delta_{\mathrm{CL}}) = 0 \tag{18}$$

For $A_{\mathrm{em}}/A_{\mathrm{e}} = A_{\mathrm{i}}/A_{\mathrm{e}} = \pi/2$, and for $d \cong \lambda_{\mathrm{De}}$ ($k \cong 1$), the solution of this equation delivers $\Delta_{\mathrm{CL}} \cong 0.7$. This means that the floating potential of the emissive probe saturates $0.7 k_{\mathrm{B}} T_{\mathrm{e}}/e$ below the true value of the plasma potential. This is due to the formation of a virtual cathode inside the probe sheath. A similar drop of the floating potential on the order of $T_{\mathrm{e}}$ has been derived in [14], using a more sophisticated approach. We point out that this effect is practically independent of the ion mass.

## 4. Experimental set-up

The emissive probe (see figure 1) used for the potential measurements in the CASTOR tokamak consists of a ceramic tube ($Al_2O_3$) with an oval cross-section of 1.4/2.3 mm outer diameter and a length of 8 cm. The $Al_2O_3$ tube has two bores of 0.7 mm diameter each, through which a 0.2 mm diameter tungsten wire is inserted in such a way that on one side of the tube (at the 'hot end') a tungsten wire loop of an approximate total length of 6 mm is formed. Inside the bores,

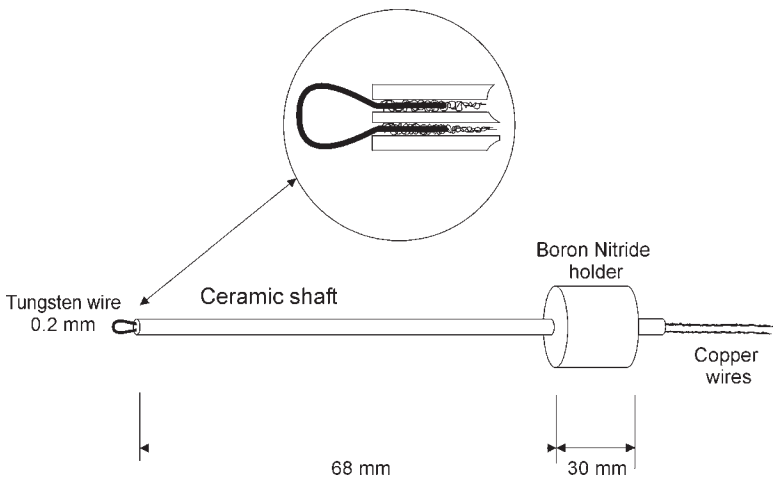


**Figure 1.** Schematic of the emissive probe head used for measurement on the CASTOR tokamak.

the tungsten wire extends at least 5 cm towards the other end (the 'cold end') of the ceramic tube. Before the insertion, each tungsten wire is spliced twice with about 18–20 copper threads with diameters of 0.05 mm [8]. In this way, inside the bores the tungsten wires are densely covered with a thin layer of copper so that the conductivity of these parts is increased.

The wrapping of the tungsten wires with copper threads is done in such a way that the electrical and mechanical contact between the tungsten and the copper is very good. The contact is further improved by the roughness of the tungsten wire and the softness of the copper. By a careful choice of the number of copper threads by which the tungsten wire is wrapped, the thickness of the combined wire can be adjusted so that it tightly fits into the bores of the $Al_2O_3$ tube. This provides an excellent electrical and mechanical contact between the two materials, which can otherwise not be soldered or welded together. On the cold end of each tube, only the spliced copper wires are protruding and can there be connected easily to any further electrical lead. Figure 1 shows a drawing of the emissive probe.

This construction has the effect that only the exposed loop of the emissive probe is heated when a current is passed through the probe wire. The total resistance of such a probe is about 0.11 Ω. The plane of the probe loop is directed parallel to the magnetic field, thus minimizing the Lorentz force on the loop wire.

In order to maximize the lifetime of the probe wire, the probe heating current was only turned on a few seconds before each shot and was kept constant until the end of the discharge. The wire attained a temperature of about 2900 K. This was calculated from the experimentally determined emission current $I_s$ (see below) and confirmed roughly by an optical pyrometer.

The CASTOR tokamak has a major radius of 0.40 m and a minor radius of $a = 85$ mm, the latter being determined by a poloidal ring limiter. The background pressure was smaller than $10^{-4}$ Pa. Before each discharge, the chamber was filled with hydrogen up to a pressure of around $10^{-2}$ Pa. The typical duration of each shot was 30 ms. The toroidal magnetic field was 1 T, and the toroidal plasma current was typically 10 kA. The typical line average plasma density was $10^{19}\,\mathrm{m}^{-3}$. In the SOL the plasma density was $0.5\text{–}2 \times 10^{18}\,\mathrm{m}^{-3}$, and $T_e$ was on the order of 10 eV.

Figure 2 shows the experimental arrangement in the CASTOR tokamak schematically. The emissive probe is mounted on a manipulator by which it can be shifted radially on a shot-to-shot basis in the range of radii $50 < r < 100$ mm. Also visible there is the position of the biasing electrode.

## 5. Experimental results and discussion

A sinusoidal sweep voltage $V_p$ with the amplitude up to ±100 V with a frequency of 1 kHz was applied to the probe during the stationary phase of the tokamak discharge. About 20 probe characteristics were recorded in each discharge with a sampling rate of 1 MHz.

Figure 3 shows three typical characteristics of the emissive probe: without heating and for two heating currents. The ion saturation current and the emission current are positive in this diagram. It is clearly seen from the figure that the left-hand branch (i.e. the ion branch) of the characteristic is strongly increased by the electron emission. The solid lines are least-square fits of the experimental points with the following function:

$$I_p(V_p) = I_s G(V_p) \left\{ 1 - \exp\left[ \frac{e(V_p - V_{fl}^*)}{k_B T_e} \right] \right\}. \tag{19}$$

The asterisk in this equation and hereafter will denote the experimentally obtained values of the floating potential and of other quantities.

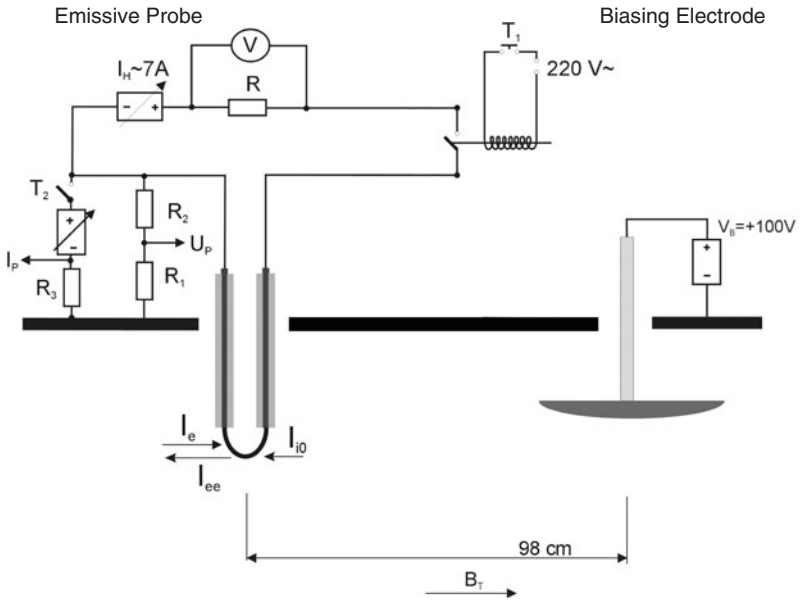


**Figure 2.** Experimental arrangement of the radially movable emissive probe in the CASTOR tokamak.

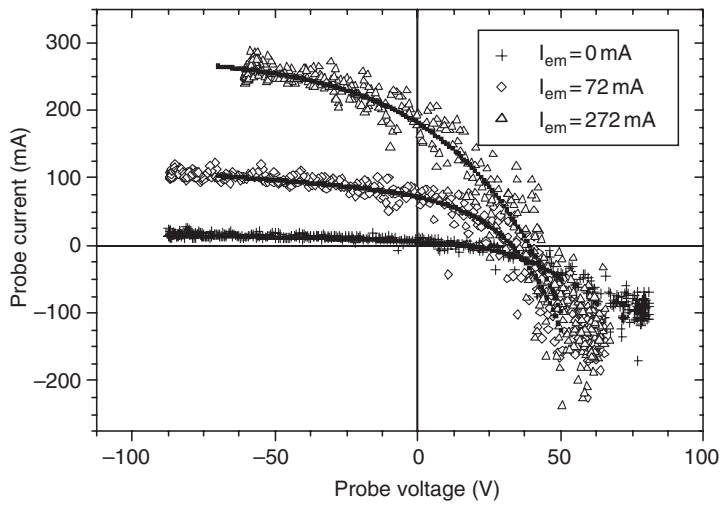


**Figure 3.** Three typical probe characteristics, taken with the cold probe and the emissive probe at two different heating currents. The solid lines are fits of the characteristics by equation (19).

The *ad hoc* multiplying factor $G(V_p) = 1 - c[e(V_p - V_{fl}^*)/k_B T_e]^\alpha$ is phenomenological, and describes the non-saturation of the ion branch of the experimentally observed probe characteristics. It is worth noting that the value of the exponent $\alpha$ is not critical, and we used $\alpha = 1.5$. Equation (19) is a four-parameter ($I_s$, $c$, $V_{fl}^*$, $T_e$) fitting function. The parameter $I_s$ represents the sum of the ion saturation current $I_{is}$ and the emission current $I_{em}^*$ at the floating potential, where we suppose that this value is constant for $V_p < V_{fl}^*$. The fit was performed up to voltages slightly above the floating potential, thus neglecting the electron saturation part

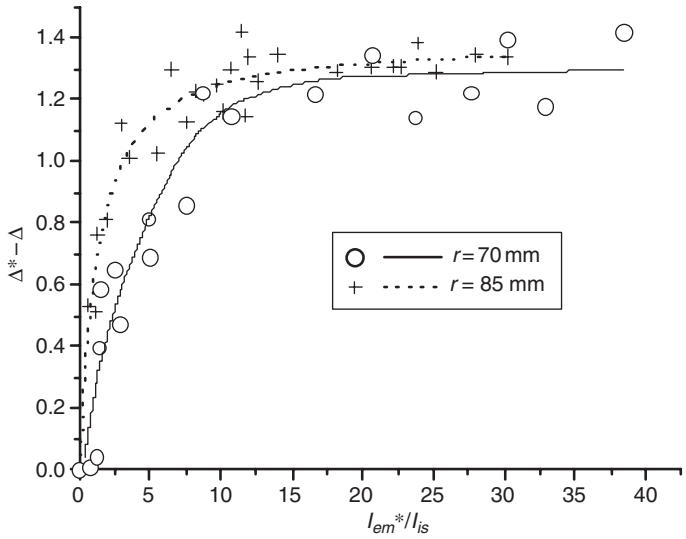


**Figure 4.** Plot of the quantity $\Delta^* - \Delta$, which represents $e(V_{\rm fl}^* - V_{\rm fl})/k_{\rm B}T_{\rm e}$, versus the normalized emission current $I_{\rm em}^*/I_{\rm is}$ for two radial positions of the probe: the crosses are for the SOL ($r = 85$ mm), and the open circles are for the confined plasma ($r = 70$ mm).

of the characteristic. Although the electron temperature was obtained for each value of the emission current $I_{\rm em}^*$, only the value $T_{\rm e}$ for the non-heated probe ($I_{\rm em}^* = 0$) was used for further processing. The measured values of $T_{\rm e}$ from 10 to 15 eV agreed well with previous Langmuir probe measurements in the CASTOR tokamak [16]. An estimate of the emission current has been obtained by taking $I_{\rm is}$ at $I_{\rm em}^* = 0$.

In figure 4 the quantity $\Delta^* - \Delta$, which represents $e(V_{\rm fl}^* - V_{\rm fl})/k_{\rm B}T_{\rm e}$, is plotted as a function of the normalized emission current $I_{\rm em}^*/I_{\rm is}$ for two radial positions of the probe. In agreement with equation (10) the quantity $\Delta^* - \Delta$ rises steeply at small emission currents, and finally reaches saturation. As we see, the normalized difference between the floating potential of the cold probe $V_{\rm fl}$ and its saturated value $V_{\rm fl,sat}^*$ amounts to $1.3k_{\rm B}T_{\rm e}/e$. Moreover, the saturation is reached for an emission current on the order of ten times the ion saturation current.

As an illustration of its applicability as an edge plasma diagnostic tool in magnetic confinement devices, the emissive probe has been used in CASTOR under different discharge conditions. The radial profile of the saturated floating potential of the emissive probe $V_{\rm fl,sat}^*$ was measured not only in Ohmic discharges, but also in regimes where the radial electric field at the plasma edge was modified by a biased electrode [17]. As an example, figure 5 demonstrates the experimentally obtained radial profiles of $V_{\rm fl,sat}^*$ (with respect to the wall) both for Ohmic and biased conditions. The biasing electrode was located at $r = 73$ mm, which corresponds to the position of the last closed flux surface, and was biased with respect to the wall to +100 V. In agreement with our previous experiments, the gradient of the potential is modified not only between the electrode and the wall, but also in front of the electrode (separatrix biasing). The radial electric field during biasing increases up to $E_{\rm r} \cong -10\,{\rm kV\,m^{-1}}$.

## 6. Discussion

We successfully performed measurements with an emissive probe in the edge region of the CASTOR tokamak, both inside and outside the last closed flux surface. The use of an

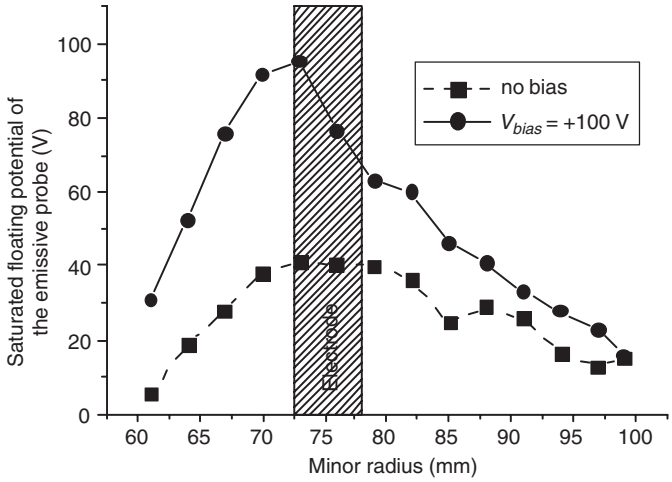


**Figure 5.** Radial profile of the plasma potential in the edge region of the CASTOR plasma in the Ohmic (■) and polarized phases (●) of the discharge (the biasing electrode is positioned at $r_b = 75$ mm and biased to $V_b = +100$ V).

emissive probe has allowed us to check the standard Langmuir theory and to show that the simple interpretation of its floating potential as the plasma potential may not be straightforward. In fact, the saturated normalized difference $\Delta^* - \Delta$ between the floating potential of an emissive probe and of a cold probe was experimentally found to be 1.3 (see figure 4). This is smaller than predicted by the simple theory in equation (7) (without space charge effect), which has yielded 2.04, under the assumption that the saturated value corresponds to the plasma potential. There are a number of effects which might shift the floating potential of the cold probe upwards, thereby reducing the difference $\Delta$ (=2.04) following from the simple theory. These effects are listed and discussed below undercases (a)–(f).

On the other hand, by taking into account space charge effects, the measured value of $\Delta^* - \Delta = 1.3$ would be in agreement with the estimates in section 3.2. In this case the saturated value $\Delta^*$ would correspond to $-\Delta_{CL}$. Thus, we cannot be sure how the saturated value observed in figure 4 is related to the true value of $\Phi$.

Figures 6(*a*) and (*b*) demonstrate the difference between these two models by schematically presenting $\Delta_{em}$ versus the emission current normalized to the ion saturation current. Thus, both figures can be compared to figure 4. Note, however, that in figures 6(*a*) and (*b*) the origin of the $y$-axis is taken at the plasma potential, while in figure 4 it is put at the floating potential of the cold probe. Figure 6(*a*) presents three possible cases without space charge effect:

- The dotted line corresponds to the case for equal collecting areas for electrons and ions, i.e. $A_e/A_i = 1$, and thus $\Delta = 2.49$ and $I_{es}/I_{is} \cong 12$ (equation (7)).
- In the case of the solid line, $A_e/A_i \cong 2/\pi$ and thus $\Delta = 2.04$ and $I_{es}/I_{is} \cong 7.7$ (equation (7)).
- The dashed line presents the case (also for $A_e/A_i \cong 2/\pi$) where the combined influence of all effects (a)–(f) (listed below) that can lead to a shift of the cold probe floating potential is taken into account. Here we find that $\Delta \cong 1.4$ and $I_{es}/I_{is} \cong 4$.

Figure 6(*b*) schematically presents $\Delta_{em}$ for the space charge case only, where it is found that the saturated floating potential of the probe is shifted downwards by $\Delta_{CL} \cong 0.7$. We emphasize that in figure 6(*b*) the saturation of $\Delta_{em}$ sets in already at $I_{em}/I_{is} \cong 5$. The dashed

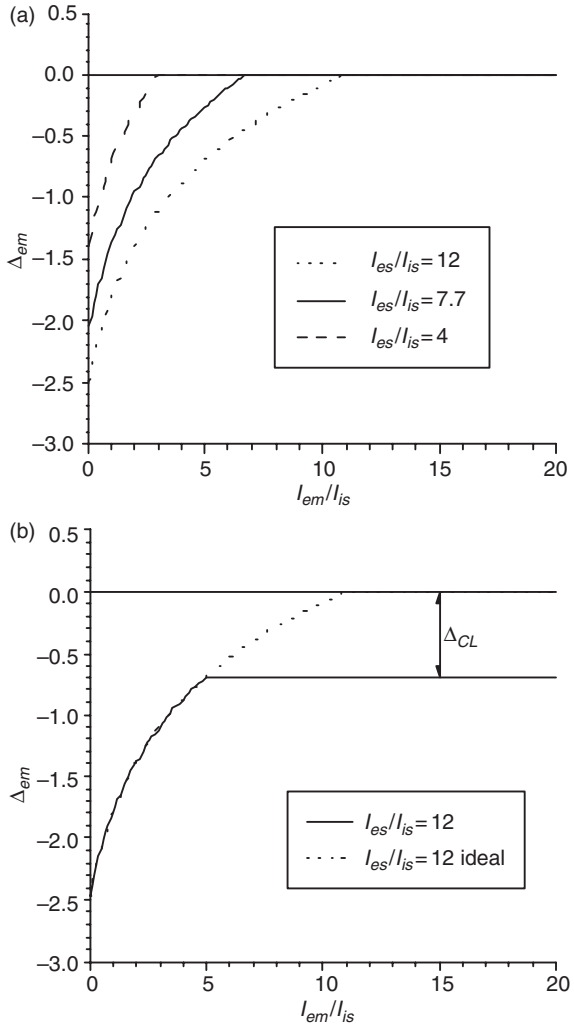


**Figure 6.** Theoretical difference between the plasma potential and the floating potential of an emissive probe, normalized to the electron temperature, plotted versus the electron emission current, normalized to the ion saturation current. (*a*) No space charge effects: dotted line for $A_e = A_i$, thus $\Delta = 2.48$ and $I_{es}/I_{is} = 12$, saturation starts at $I_{em}/I_{is} = 11$; solid line for $A_e/A_i = 2/\pi$, thus $\Delta = 2.04$ and $I_{es}/I_{is} = 7.7$, saturation starts at $I_{em}/I_{is} = 6.7$ (equations (11) and (12)); the dashed line is taking account of the shift of the cold probe floating potential due to the effects listed in section 6 under (a)–(f); this reduces $\Delta$ to about 1.4 and $I_{es}/I_{is}$ to about 4 and $I_{em}/I_{is} = 3$ where saturation starts. (*b*) Taking into account space charge effects of the emitted electrons: in this case the saturated value of $\Delta_{em}$ does not reach the plasma potential but remains below by $\Delta_{CL} \cong 0.7$; saturation starts for $I_{em}/I_{is} \cong 4$.

line in figure 6(*a*) saturates even already for $I_{em}/I_{is} \cong 3$, the solid line at $I_{em}/I_{is} \cong 6.7$, and the dotted line at $I_{em}/I_{is} \cong 11$.

The following effects can influence the floating potential of a cold probe in a hot magnetized plasma:

*(a) Secondary electron emission caused by plasma electrons impacting on the probe surface:* The secondary electron emission from the probe surface induced by impinging plasma electrons

shifts the floating potential upwards by the amount $\ln(1-\gamma_e)$, as is evident from equation (3). According to [18], the secondary electron emission coefficient of tungsten (the material used for the present experiments) for 100 eV monoenergetic electrons would be of the order of 0.3. This would give a reduction of $\Delta$ (compared to $\Delta$ at $\gamma = 0$) by 0.36. Pitts and Matthews [19] measured the value of $\gamma_e$ under a realistic electron energy distribution function and in a strong magnetic field with normal incidence to a molybdenum surface, and found it to be close to one. However, this would reduce $\Delta$ to almost zero, so that the cold probe would automatically be at the plasma potential. This obviously contradicts our experimental observation, since we do observe a reduction of $\Delta$ with increasing thermal electron emission.

*(b) Secondary electron emission caused by plasma ions impacting the probe surface:* Plasma ions can also give non-negligible secondary electron emission, although this effect is usually not taken into account in tokamak probe diagnostics. For 100 eV monoenergetic protons impinging on several types of metal, the secondary emission coefficient $\gamma_i$ has been measured to be as high as 0.2 [20]. Pitts and Matthews [19] also obtain a similar number for a realistic ion energy distribution acting on molybdenum. This gives a reduction of $\Delta$ by 0.18.

*(c) Ion temperature:* Measurements of $T_i$ in the tokamak edge are seldom available, but investigations in other comparable tokamaks [19,21] indicate that sometimes $T_i$ might be higher than $T_e$. If we assume $T_i > T_e$ by a factor of four, equation (6) predicts a decrease of $\Delta$ by 0.45.

*(d) Impurities:* The assessment of the contribution of impurities to the difference $\Delta^* - \Delta$ is negligible as compared to the other effects discussed here. A detailed analysis can be found in [22].

*(e) Electron and ion drifts:* The presence of plasma flows can affect the value of the floating potential [10, 23]. The same will happen in the case of a parallel flow of electrons, which will distort the electron distribution function from the Maxwellian shape and alter the electron current collected by the probe [24]. The impact of such effects can be hardly estimated without a knowledge of the Mach number and of the form of the electron distribution function.

*(f) Different collecting areas for electrons and ions (further considerations):* Due to the complicated geometry of the emissive probe, the effective collecting area for electrons can even be smaller than $A_e = 4r_p l_p$, whereas that for ions would not be affected. However, those electrons impinging on the probe near the top where the loop has its strongest curvature only partly graze the probe surface and therefore contribute less to the total electron current. Moreover, in the same region the wire surface inside the loop is not accessible for all electrons since it is partly shaded. Therefore $A_e < 2A_i/\pi$. As mentioned above, in the most extreme case, when the loop is exactly parallel to $\boldsymbol{B}$, $A_e = A_i/\pi$. Such an effect reduces the normalized difference $\Delta$, which for the latter case attains even a value of 1.34. This would agree very well with the experimentally observed value.

## 7. Conclusion

The above discussion shows that there are several reasons, because of which the difference between the potential of the emissive and the cold probe is only 1.3 times the electron temperature, which is less than the canonical value 2.04 predicted by the probe theory. This discrepancy could be explained either by space charge effects or by a number of effects discussed above. Additional experiments will be performed to distinguish between these two possibilities.

In spite of the fact that the interpretation of our experiments is not yet definitive, we have already started to use the emissive probes for fluctuation measurements.

## Acknowledgments

Two of the authors (C I and R S) would like to thank the Institute for Plasma Physics of the Czech Academy of Science in Prague, Czech Republic, for the hospitality extended to them on the occasion of their visit. This work was carried out within the Association EURATOM/ÖAW, within the Association EURATOM/ENEA and within the Association IPP.CR under contract. The content of the publication is the sole responsibility of the authors and does not necessarily represent the views of the Commission or its services. Support by the Fonds zur Förderung der wissenschaftlichen Forschung (Austria) under Grant No P-14545 and by the University of Innsbruck and by the Grant Agency of the Czech Republic Grant No 202/00/1217 are also acknowledged.

## References

[1] van Oost G 2000 *J. Tech. Phys.* **41** 41
[2] Endler M, Niedermeyer H, Giannone L, Holzbauer R, Rudyj A, Theimer G, Tsois N and the ASDEX Team 1995 *Nucl. Fusion* **35** 1307
[3] Stangeby P C 1982 *J. Phys. D: Appl. Phys.* **15** 1007
[4] Hutchinson I H 1987 *Principles of Plasma Diagnostics* (Cambridge: Cambridge University Press)
[5] Kemp R F and Sellen J M Jr 1966 *Rev. Sci. Instrum.* **37** 455
Smith J R, Hershkowitz N and Coakley P 1979 *Rev. Sci. Instrum.* **50** 210
[6] Motley R W 1972 *J. Appl. Phys.* **43** 3711
Fujita H and Yagura S 1983 *Japan. J. Appl. Phys.* **22** 148
[7] Iizuka S, Michelsen P, Rasmussen J J, Schrittwieser R, Hatakeyama R, Saeki K and Sato N 1981 *J. Phys. E: Sci. Instrum.* **14** 1291
[8] Siebenförcher A and Schrittwieser R 1996 *Rev. Sci. Instrum.* **67** 849
[9] Makowski M A and Emmert G A 1983 *Rev. Sci. Instrum.* **54** 830
[10] Schrittwieser R, Avram C, Balan P C, Cabral J A, Figueiredo F H, Pohoaţă V and Varandas C 2001 *Contrib. Plasma Phys.* **41** 494
[11] Hershkowitz N, Nelson B, Pew J and Gates D 1983 *Rev. Sci. Instrum.* **54** 29
[12] Richardson O W and Young A F A 1925 *Proc. R. Soc.* A **107** 377
[13] Reinmüller K 1998 *Contrib. Plasma Phys.* **38** 7
[14] Ye M Y and Takamura S 2000 *Phys. Plasmas* **7** 3457
[15] Chen F F 1984 *Introduction to Plasma Physics and Controlled Fusion Vol 1: Plasma Physics* 2nd edn (New York: Plenum) p 294
[16] Gunn J, Stöckel J, Adámek J, Ďuran I, Horáček J, Hron M, Jakubka K, Kryška L, Žáček F and van Oost G 2001 *Czech. J. Phys.* **51** 1001
[17] van Oost G, Stöckel J, Hron M, Devynck P, Dyabilin K, Gunn J, Horáček J, Martines E and Tendler M *Proc. 11th Int. Toki Conf. on Plasma Physics and Controlled Nuclear Fusion (ITC-11) (Toki, Japan, 2000) J. Plasma Fus. Res. Ser.* vol 4
[18] Gibbson D J 1966 Secondary electron emission *Handbook of Vacuum Physics Vol 2: Physical Electronics* ed H Beck (London: Pergamon) p 301
[19] Pitts R A and Matthews G F 1990 *J. Nucl. Mater.* **176&177** 877
[20] Kislyakov A I, Stöckel J and Jakubka K 1976 *Sov. Phys.-Techn. Phys.* **20** 986 (1975 *Zh. Tekh. Fiz.* **45** 1545)
[21] Matthews G F, Pitts R A, McCracken G M and Stangeby P C 1991 *Nucl. Fusion* **31** 1495
[22] Stangeby P C 1987 *J. Phys. D: Appl. Phys.* **20** 1472
[23] Jachmich S, Van Goubergen H and Weynants R 2000 *Proc. 27th EPS Conf. on Controlled Fusion and Plasma Physics (Budapest, Hungary, 2000) Europhys. Conf. Abstr.* **24B** 832
[24] Stangeby P C 1995 *Plasma Phys. Control. Fusion* **37** 1031